Hindawi
Advances in Civil Engineering
Volume 2020, Article ID 4974082, 18 pages
https://doi.org/10.1155/2020/4974082

Research Article

The Wind Loading Characteristics of MAN Type Dry Gas Storage Tank

Xinpeng Liu,[1,2] **Zhitao Yan**,[1,2] **Zhengliang Li**,[2,3] **Junfan Chen**,[1] **and Jingbo Liu**[1]

[1]*School of Civil Engineering and Architecture, Chongqing University of Science & Technology, Chongqing, China*
[2]*Chongqing Key Laboratory of Energy Engineering Mechanics & Disaster Prevention and Mitigation, Chongqing, China*
[3]*School of Civil Engineering, Chongqing University, Chongqing, China*

Correspondence should be addressed to Zhitao Yan; 2017001@cqust.edu.cn

Received 23 September 2019; Revised 12 December 2019; Accepted 4 January 2020; Published 20 February 2020

Academic Editor: Castorina S. Vieira

The effects of Reynolds number (Re) and surface roughness on the wind pressure coefficient on a MAN type dry gas tank were analyzed in detail by wind tunnel tests. A wind load calculation model was then established, which is suitable for the wind resistant design of the gas tanks. The test results revealed that in the range of $7 \times 10^5 < \mathrm{Re} < 1.0 \times 10^6$ (supercritical regimes), the drag coefficient (C_d) and wind pressure coefficient remained constant, consistent with 2D cylinders in a uniform flow. However, in common with 2D cylinder flows, the surface roughness with the spacing ratio (λ) greater than 0.9 had a significant effect on the wind pressures coefficient. The minimum pressure coefficient ($C_{p\min}$) sharply increased from −2.3 to −0.65 with increasing surface roughness. The corresponding angle for the minimum pressure coefficient $\theta_{\min}$ was in between 140°and 90°, which was in a gradual decreasing trend with the increase in surface roughness of the model. The calculation method of the wind pressure coefficient with vary surface roughness was proposed, based on which, the calculation results were in good agreement with the test data.

1. Introduction

Gas tank is an important industrial structure. This structure is mainly made up of tank dome, cylindrical cabinet, internal piston, and supporting members. As shown in Figure 1, the gas tank is a simple circular cross-section structure. When it comes to aerodynamics, simple circular cross-section always brings a complex behavior [1], as the features of flow separation strongly depend on Reynolds number. The aerodynamics of circular cylinders is characterized by abrupt transitions in the flow pattern and in the force parameters, depending only on Reynolds number and defining the aerodynamic regimes. The aerodynamic regimes and the related flow characteristics around a circular cylinder are shown in Table 1.

With the variety of Reynolds number, the development of flow transition around a cylinder experiences three states: wake transition (TrW), shear layer transition (TrSL), and boundary layer transition (TrBL). In Eiffel's [8] study of spheres in the air, it was found that when Re = 120, the resistance of spheres would suddenly decrease. Wieselsberger [2] explained that the sudden drop of resistance was related to the transition of the boundary layer near the separation point. Taylor [9] first reported the average pressure distribution on the surface of a cylinder in the TrBL state. Fage and Johansen [10] carried out more detailed experimental studies and found a very complex coupling phenomenon between transition and separation. Cantwell [11] repeated the average pressure distribution measurements test in TrBL states. The test results show that the minimum pressure coefficient decreases sharply with the increase of the Reynolds number. Korotkin [12] took a short cylinder with end plates as the research object and simultaneously tested the surface pressure distribution of the cylinder at 35 positions. The experimental results showed that the local bubble rupture had a significant effect on the pressure coefficient distribution. Roshko [5], Schmidt [13], Jones and Knudsen [14], and Warschauer and Leene [15] tested the reference pressure of a cylinder in the transcritical region. Due to the breakdown of separated bubbles, the

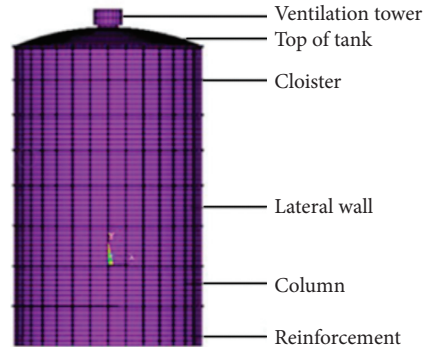

Figure 1: Geometry model of the gas tank.

Table 1: Aerodynamic regimes and flow characteristics around a circular cylinder. Data from Wieselsberger [2]; Schewe [3]; Williamson [4]; Roshko [5]; Norberg [6]; Demartino and Ricciardelli [7].

Regime	No separation	Pair of stationary vortex	Laminar vortex shedding	Turbulent vortex shedding
Re range	$0 < \mathrm{Re} < 5$	$0 < \mathrm{Re} < 5$	$0 < \mathrm{Re} < 5$	$0 < \mathrm{Re} < 5$
C_d	$\infty > C_d > 4$	$4 > C_d > 2.1$	$2.1 > C_d > 1.5$	$1.5 > C_d > 1.3$
C_l	0	0	0	0
St	—	—	$0.1 < \mathrm{St} < 0.2$	$0.2 \cong \mathrm{St} \cong 0.2$
Sketch	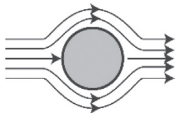	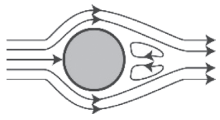	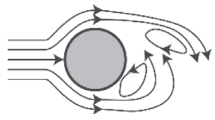	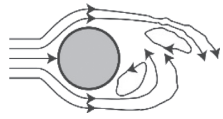
Regime	Subcritical	Critical	Supercritical	Transcritical
Re range	$300 < \mathrm{Re} < 3 \times 10^5$	$3 \times 10^5 < \mathrm{Re} < 3.5 \times 10^5$	$3.5 \times 10^5 < \mathrm{Re} < 4.5 \times 10^6$	$4.5 \times 10^6 < \mathrm{Re} < \infty$
C_d	$1.3 > C_d > 1.2$	$1.2 > C_d > 0.3$	$0.3 < C_d < 0.5$	$C_d > 0.5$
C_l	0	$\cong 1.3$	0	0
St	$0.2 \cong \mathrm{St} \cong 0.2$	$0.2 < \mathrm{St} < 0.45$	$0.45 > \mathrm{St} > 0.25$	$\mathrm{St} < 0.25$
Sketch	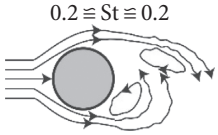	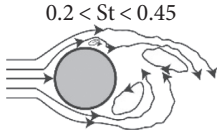	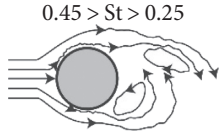	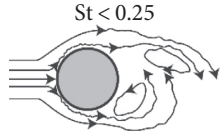

experimental data points showed very large dispersion. In addition, Roshko [5] revealed a high Reynolds number transition in which the drag coefficient changed dramatically, which indicated the effect of Reynolds number on the drag coefficient of the circular cylinder was significant. Through reconfirming Roshko's [5] experimental results, Achenbach [16] measured the local pressure and skin friction distribution around the cylinder. From the results the total drag, the pressure drag, and the friction drag were calculated. According to the skin friction distribution, the position of the separation points, separation bubbles, and transition points can be localized, which allow one to define three typical states of the flow. Bearman [17] found that onset of mean lift force caused by a one-side separation from one side of the cylinder. Although there was agreement about the flow features around a circular cylinder depending on the Reynolds number, the description about steps by which the transition from laminar to turbulent occurs was not understood until four regimes were proposed by Achenbach [18].

On the other hand, surface irregularities, commonly termed roughness, are another important factor affecting aerodynamic characteristics of the circular cylinder. Pioneering experiments on the effects of uniform roughness on the aerodynamics of circular cylinders in cross flow were performed by Fage and Warsap [19]. They determined C_d for $2.5 \times 10^4 < \mathrm{Re} < 2.5 \times 10^5$ and for $5 \times 10^{-4} \leq \mathrm{Re} \leq 2 \times 10^{-2}$. It was observed that in the subcritical regime roughness has no influence on C_d, while in the supercritical regime C_d increases with increasing k/D. The most significant differences are in the critical regime, where the minimum value of C_d increases and R_{ec} decreases with increasing k/D. It was observed that in the subcritical regime roughness has no influence on C_d, while in the supercritical regime C_d increases with increasing k/D. The most significant differences are in the critical regime, where the minimum value of C_d increases and R_{ec} decreases with increasing k/D. To better understand the effects of roughness on the boundary layer over a circular cylinder with uniform roughness, different researchers measured surface pressures and shear stresses.

Similarly to smooth cylinders, in the range $4 \times 10^4 < \mathrm{Re} < 3 \times 10^6$, for the rough cylinders, shear stresses contributed only a few percent to the total drag [18]. In the case of rough cylinders, Buresti [20] defined the critical regime as the absence of regular vortex shedding, the upper transition regime as the appearance of vortex shedding, and postcritical regime as the independence of St and C_d on Re. In the subcritical regime, separation was found to be laminar and to occur in the front portion of the cylinder, as a consequence of the shear stresses [18]. However, the transition boundary between subcritical and critical is strongly affected by roughness, which was pointed out by Achenbach [18]. The strongest influence of roughness occurs in the critical regime, where roughness itself is the cause producing local turbulence, as it inhibits the formation of the separation bubble and hence obliterates the one and two bubble regimes [21]. Ribeiro [22] studied the roughness generated by ribs, wire mesh screen, and sand paper and demonstrated that variety of roughness textures produced major changes of roughness, even the same physical scale. After reviewing a large amount of investigations on the flow features around a circle cylinder, Zdravkovich [23] presented a relationship between C_d and Re, by which the variation of C_d against Re has been well described in a range of Re up to over 10^7. Moreover, it is well known that the onset of surface roughness has evident affect to the typical flow features, Achenbach and Heinecke [24] revealed the differences between the Reynold number regimes for rough and smooth surfaces. Zou et al. [25] proposed a new definition of surface roughness (k/s) and a conversion formula with the original definition of surface roughness. Cheng et al. [26] carried out a pressure measurement experiment of the cooling tower in the uniform flow field and atmospheric boundary layer respectively, in which surface roughness effects on both static and dynamic wind loads were studied and quantified.

As discussed above, there were a large number of studies on the aerodynamic characteristics of a single circular cylinder, but there are few research studies concerning the effect of Re and surface roughness on flow features and wind pressure distribution of the gas tank.

In this paper, the effects of the Re and surface roughness on the wind characteristic of the gas tank has been investigated by the wind tunnel test. Based on the analytical results, the wind load calculation method for the gas tank structure was proposed for the first time. This calculation method could be widely used in the wind resistance design of the gas tank structure.

2. Wind Tunnel Experiment

2.1. Overview of the Experiment. To understand wind pressure distributions, the whole gas tank is simplified into the tank dome, the cylindrical cabinet, and the supporting members. In order to simulate the real Re characteristics of the gas tank [27, 28] as much as possible, the geometrical scale of the gas tank rigid model was determined to be 1/50.

The total height (L) and diameter (D) of the model are 2.4 m and 1.32 m, respectively. The radius of curvature of the dome is 1.76 m. The corresponding rigid model is shown in Figure 2.

There were 416 pressure measurement points arranged on the rigid model. Eleven layers of measurement points were set up along the height of the model, spaced 180 mm apart. Thirty-two measurement points were arranged evenly along the circumferential direction at each layer. The layout and geometric design dimensions of the model are shown in Figure 3.

The wind tunnel test was conducted in the uniform flow and atmospheric boundary layer (ABL) turbulent flow field of Type A according to Chinese Codes, respectively. The longitudinal integral scale is about 0.9 m~1.8 m. The simulation results of Type A wind field are listed in Figure 4.

2.2. Experiment Cases. For each experiment case, pressure measurement tests in both uniform and Type A flow fields were conducted with different 5 test reference wind speeds 4.5 m/s, 6 m/s, 7.6 m/s, 9.2 m/s, and 10.5 m/s. The corresponding Re are 4.0×10^5, 5.5×10^5, 7.0×10^5, 8.4×10^5, and 9.6×10^5.

2.2.1. In the Uniform Flow. To compare with the results of the previous literature, the smooth circular cylinder rigid model was placed on the center turntable of the test section, and the wind pressure measurement experiment was conducted with different 5 reference wind speeds.

To study the surface roughness effects, different 9 surface roughness (γ) which would be defined below were simulated on the model by sticking rough strips. The height range of the rough strip was 1–6 mm. The width of the rough strip was 5 mm. The experiment cases are listed in Table 2.

2.2.2. In the ABL Turbulent Flow Field. To understand the characteristic wind pressure distribution of the gas tank, the same experiments were conducted in the ABL turbulent flow field.

2.3. Experiment Equipment. The Digital Service Module and Electronic pressure scanning module were used to acquire pressure data at measurement points. Each ZOC33 module incorporates 64 individual silicon pressure sensors, calibration valving, a high-speed multiplexer (45 kHz), and an instrumentation amplifier. An integral "duplexing" valve is available to allow the ZOC33's 64 sensors to service up to 128 input pressures.

2.4. Experiment Arrangement. In order to meet the maximum of blockage requirement, the wind tunnel test was conducted in the XNJD-3 wind tunnel of Southwest Jiao Tong University. The width and height of the wind tunnel are 22.5 m and 4.5 m. The distance from the top of the model to the ceiling of the wind tunnel is 2.1 m. The maximum test wind speed is 16 m/s. The wind tunnel experiment was conducted in the uniform flow and atmospheric boundary layer (ABL) turbulent flow field of Type A according to Chinese Codes, respectively. The spires and rough elements were used to simulate the ABL turbulent field flow.

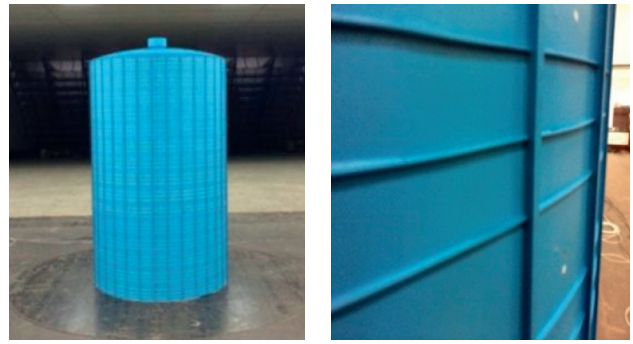

(a) (b)

Figure 2: (a) Rigid model of the gas tank. (b) Detailed model surface.

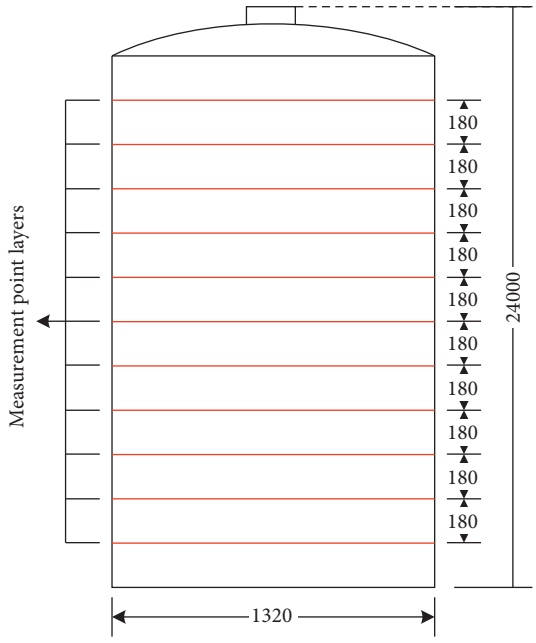

Figure 3: Layout of measurement point.

The spires were made of the isosceles triangular wood structure with height of 4.2 meters. The rough elements were made of cubic wood blocks. The lengths of one side of the large and small rough element were 0.2 m and 0.1 m. The installation of turbulent field and simulation results of wind field are shown in Figure 5.

2.5. Parameters Definition

2.5.1. Wind Pressure Coefficient. The instantaneous wind pressure coefficient of the ith measurement point on the surface of the model is given by

$$C_{p_i}(t) = \frac{p_i(t) - p_\infty(Z)}{\rho V_\infty^2(Z)/2}, \tag{1}$$

where $p_i(t)$ indicates the instantaneous surface wind pressure of the ith measurement point that is positive inwards and negative outwards, Z represents the height of the ith measurement point, $p_\infty(Z)$ and $V_\infty(Z)$ denote the freestream static pressure and oncoming air velocity at high Z, respectively, and ρ is the density of the air.

The mean wind pressure coefficient of the ith measurement point is given by

$$C_{p_i} = \frac{1}{m}\sum_{t=1}^{m} C_{p_i}(t), \tag{2}$$

where m indicates the samples number of wind pressure data.

The fluctuating wind pressure coefficient of the ith measurement point is given by

$$C_{p_{i\mathrm{RMS}}} = \left[\frac{1}{m}\sum_{t=1}^{m}\left(C_{p_i}(t) - C_{p_i}\right)^2\right]^{1/2}. \tag{3}$$

2.5.2. Characteristic Parameters of Wind Pressure Distribution. The characteristic parameters of mean wind pressure distribution on the gas tank surface are shown in Figure 6.

2.5.3. Surface Roughness. The surface roughness is given by

$$\gamma = \frac{k}{s}, \tag{4}$$

where k is average height of rough bar and s is the distance between the rough bar, which are shown in Figure 7.

3. Discussion of Experimental Result

3.1. Effect of Reynolds Number on Drag Coefficient and Minimum Pressure Coefficient. The effects of Reynolds number on the drag coefficient (C_d) and minimum pressure coefficient ($C_{p\min}$) were shown in Figures 8 and 9. For space reasons, only partial test results are listed.

3.1.1. Drag Coefficient C_d. The drag coefficient of each measurement layer of the gas tank was obtained by weighted averaging the wind pressure data of each measurement point:

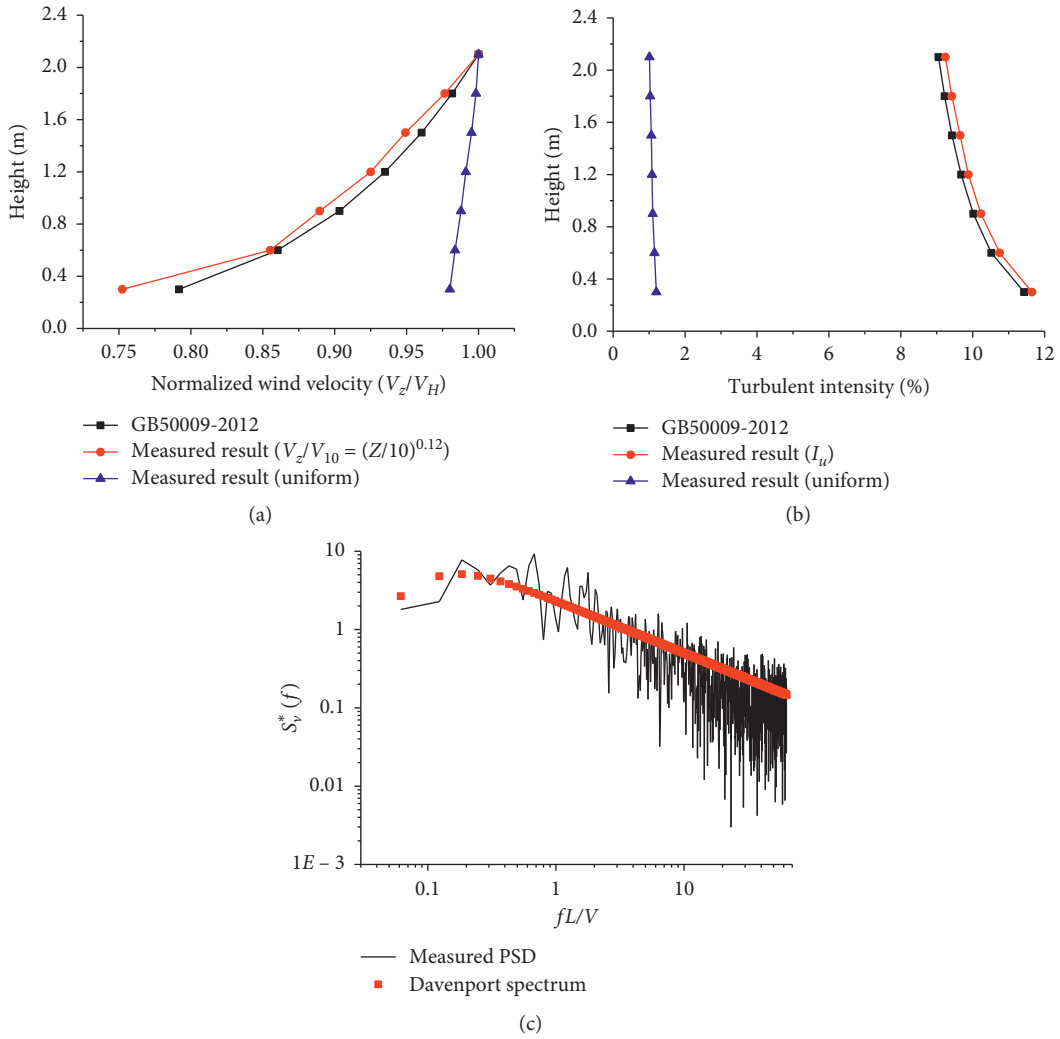

Figure 4: Simulation of Type A flow field in the wind tunnel. (a) Average wind velocity profile. (b) Turbulence intensity profile. (c) Power-spectrum function for along-wind component of wind speed.

Table 2: Relative roughness γ for different cases.

Case	Number of rough strips along the circular direction	Height of strip	Surface roughness ($\gamma = k/s$)	Wind field
U-1	0	0	0	Uniform flow
U-2	32	1	0.0077	
U-3	32	2	0.0154	
U-4	32	3	0.0231	
U-5	32	4	0.0308	
U-6	32	5	0.0386	
U-7	32	6	0.0463	
U-8	64	4	0.0617	
U-9	64	5	0.0771	
U-10	64	6	0.0926	
T-1	0	0	0	Type A turbulent flow
T-2	32	1	0.0077	
T-3	32	2	0.0154	
T-4	32	3	0.0231	
T-5	32	4	0.0308	
T-6	32	5	0.0386	
T-7	32	6	0.0463	
T-8	64	4	0.0617	
T-9	64	5	0.0771	
T-10	64	6	0.0926	

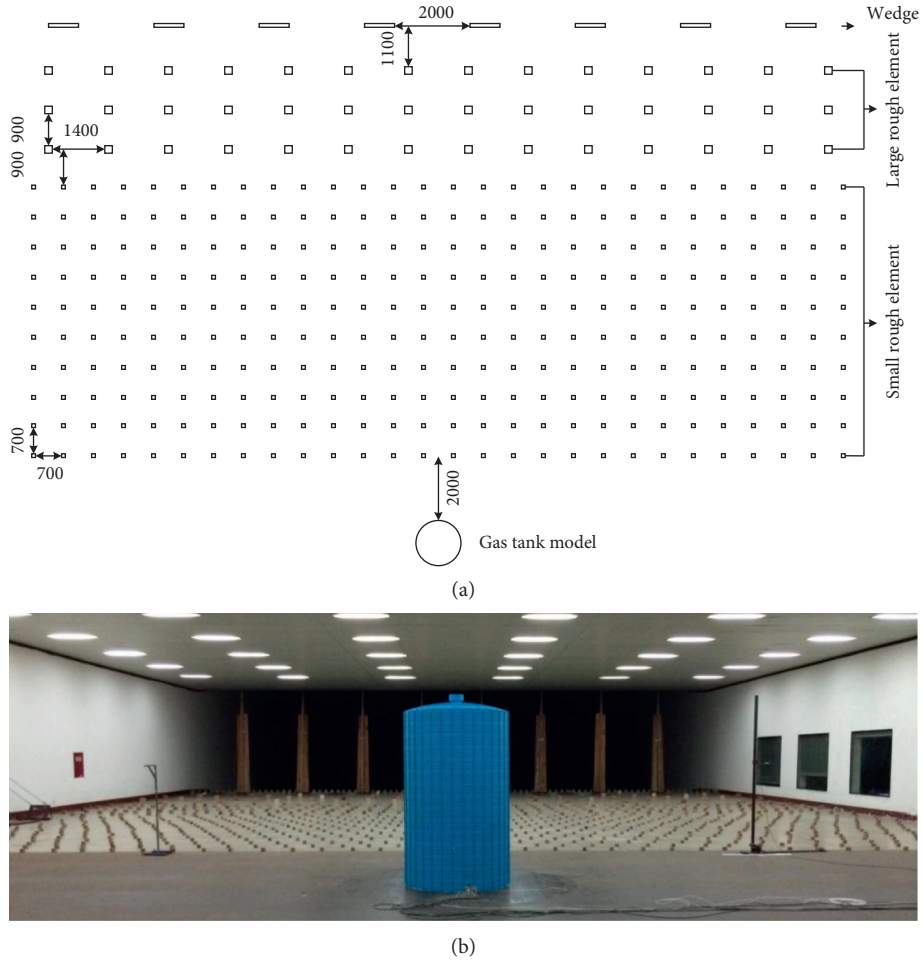

Figure 5: Arrangement of wind field. (a) Layout of turbulent field (unit: mm). (b) Realistic arrangement of turbulent field.

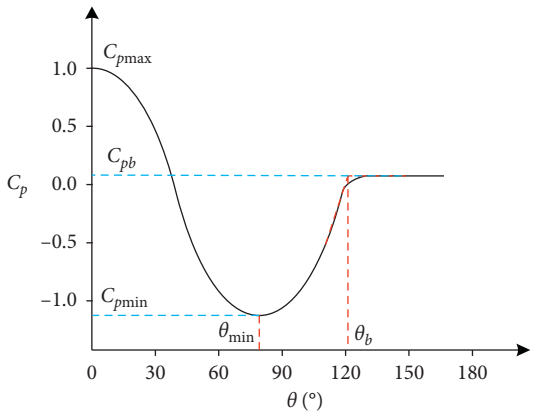

Figure 6: Definition of the characteristic parameters.

$$C_d = \frac{\pi}{N}\sum_{i=1}^{n} C_{p_i}\cos(\theta), \tag{5}$$

where θ represents the azimuthal angle of the ith measurement point and n and N represent the number of weighted average points and total points for each layer. In this section, $n = N = 32$.

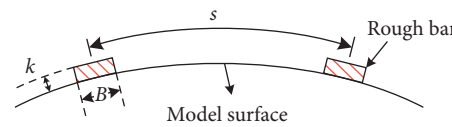

Figure 7: Diagram of surface roughness definition.

(1) Detail Results Obtained in Uniform Flow Field. Figure 8(a) shows the drag coefficient (C_d) of the gas tank model with smooth surface ($\gamma = 0$) in the uniform flow field as well as the results of the previous studies obtain from Yao et al. [29], Liu et al. [30], Güven et al. [31], and Wieselsberger [2]. When $Re < 6.0 \times 10^5$, the C_d is basically unchanged. With the increase of the Reynolds number ($6.0 \times 10^5 < Re < 1.0 \times 10^6$), the C_d increases slowly, but the trend is not significant. When $Re > 1.0 \times 10^6$, the C_d gradually kept constant. Generally, in the region of $4.0 \times 10^5 < Re < 1.0 \times 10^6$, the change of C_d of the gas tank model with the smooth surface is not significant, and the value of C_d is approximately equal to 0.3–0.35. The test results are close to those obtained by Liu et al. [30] and Wieselsberger [2]. However, the test results of C_d in this paper are smaller than those obtained by Yao et al. [29] in the whole Reynolds

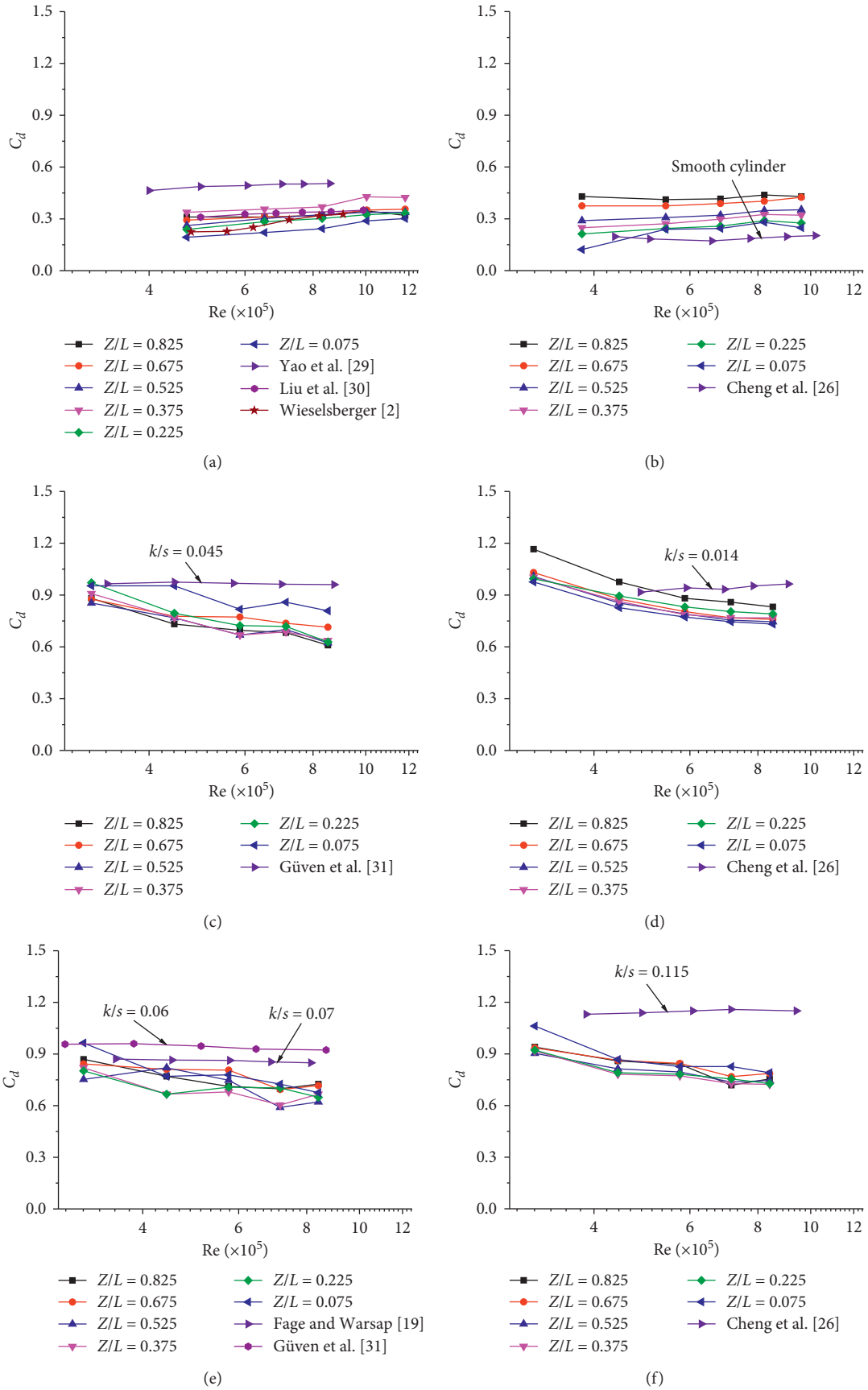

Figure 8: Effect of the Reynolds number on the drag coefficient of each measurement layer. (a, c, e) Uniform flow and (b, d, f) Type A turbulent flow field. (a, b) $\gamma = 0$, (c, d) $\gamma = 0.0386$, and (e, f) $\gamma = 0.0771$.

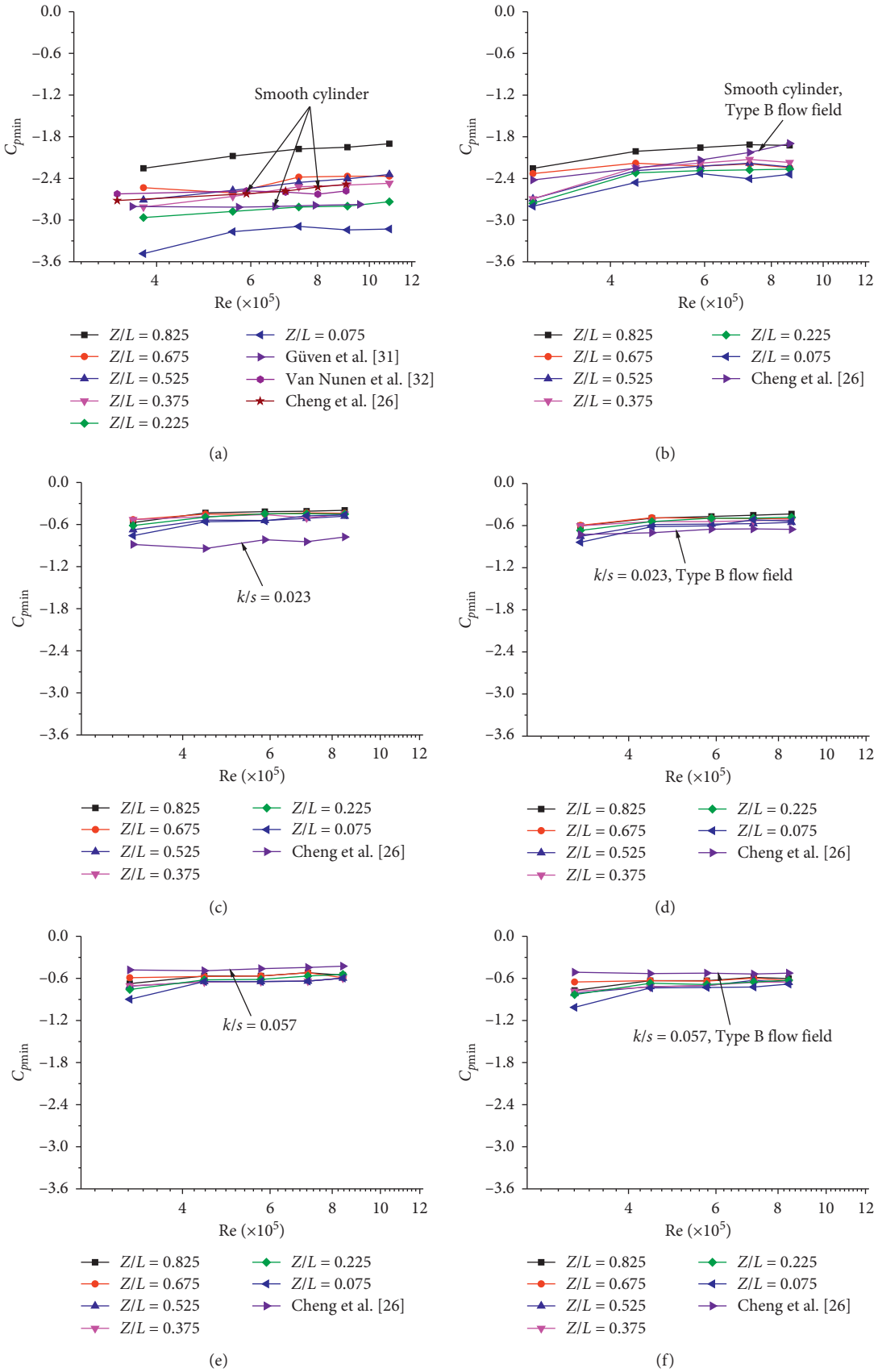

Figure 9: Effect of the Reynolds number on minimum negative wind pressure coefficient. (a, c, e) Uniform flow and (b, d, f) Type A turbulent flow field. (a, b) $\gamma = 0$, (c, d) $\gamma = 0.0386$, and (e, f) $\gamma = 0.0771$.

number region ($4.0 \times 10^5 < \mathrm{Re} < 1.0 \times 10^6$). In order to suppress the end effect of the flow field of the test model, Yao et al. [29] fixed the two square end plates on the upper and lower ends of the smooth cylindrical model. Therefore, the results of deviation are mainly caused by the three-dimensional effect of the model.

The C_d of the gas tank model with surface roughness ($\gamma = 0.0386, 0.0771$) in the uniform flow field are shown in Figures 8(c) and 8(e), respectively, and the results were compared with those obtained by Fage and Warsap [19] and Güven et al. [31]. The C_d of the gas tank model with surface roughness decreased from 0.9 to 0.7 slowly with the increase of the Reynolds number ($3.0 \times 10^5 < \mathrm{Re} < 9.0 \times 10^5$). The variety trend of C_d is almost the same in two different surface roughness. When $\gamma = 0.0386$, the C_d of this paper is smaller than those obtained by Güven et al.[31]. This is mainly due to the different surface roughness of these two tests. When $\gamma = 0.0771$, the test results in this paper are smaller than the results obtained by Güven et al. [31], but it is closer to the results obtained by Fage and Warsap [19].

(2) Detail Results Obtained in ABL. In order to further analyze the effect of the Reynolds number on C_d, the C_d of the gas tank model with the smooth surface in Type A flow field are shown in Figure 8(b) and the results were compared with those obtained by Cheng et al. [26]. Cheng et al. [26] placed a cooling tower model similar to the gas tank with different surface roughness in Type B flow field to study the wind load characteristics in this paper. It is difficult to find the same experimental results as the wind field type in this paper; therefore, the comparison of C_d between Cheng et al. [26] and this paper is still necessary. Due to turbulence, the C_d results of the smooth surface in the ABL are more dispersed than those in uniform flow. The C_d of the measurement point with different Z/L keep constant basically in the whole region of the Reynolds number ($4.0 \times 10^5 < \mathrm{Re} < 1.0 \times 10^6$). The C_d of the smooth surface in this paper are larger than those obtained by Cheng et al. [26] in the whole region of the Reynolds number. But the deviation is not significant.

The C_d of the gas tank model with surface roughness ($\gamma = 0.0386, 0.0771$) in ABL are shown in Figures 8(d) and 8(f), respectively, and the results were compared with those obtained by Cheng et al. [26]. When $\gamma = 0.0386$, the C_d of the gas tank decreased from 1.0 to 0.75 with the increase of the Reynolds number ($3.0 \times 10^5 < \mathrm{Re} < 9.0 \times 10^5$). In the region of $5.0 \times 10^5 < \mathrm{Re} < 9.0 \times 10^5$, the C_d in this paper are small than those obtained by Cheng et al. [26]. And the deviation increases in the high Reynolds number region. When $\gamma = 0.0771$, the C_d keeps constant in the whole region of the Reynolds number. The value of the C_d is approximately equal to 0.8. However, there is a deviation between the test results of this paper and Cheng et al. [26], which is mainly caused by the large difference in the surface roughness of the model.

3.1.2. Minimum Pressure Coefficient C_{pmin}

(1) Detail Results Obtained in Uniform Flow Field. Figure 9(a) shows $C_{p\min}$ results of the gas tank model with the smooth surface ($\gamma = 0$) in the uniform flow field as well as the those of previous studies obtained by Cheng et al. [26], Güven et al. [30], and Van Nunen et al. [32]. When $\gamma = 0$, the $C_{p\min}$ in the middle section of the gas tank model is close to the results obtained by et al. [26], Güven et al. [31], and Van Nunen et al. [32]. For the smooth surface model, the $C_{p\min}$ increases from −2.7 to −2.3. However, there is a deviation between the $C_{p\min}$ of the upper and lower measuring points and that of the middle measuring points, which is mainly due to the three-dimensional effect of the test.

With the increase of surface roughness, the $C_{p\min}$ of the gas tank model increases significantly to −0.7 and keep constant in the whole region of the Reynolds number, which is consist with those obtained by Cheng et al. [26]. The deviation of $C_{p\min}$ between the end and middle section of the gas tank model is not significant.

(2) Detail Results Obtained in ABL. Different from the test results in the uniform flow field, the deviation of $C_{p\min}$ on end and middle section of the gas tank model gradually decreases. When $\gamma = 0$, the $C_{p\min}$ of the gas tank model increases slowly from −2.7 to −2.4 with the increase of the Reynolds number, which is consist with the results obtained by Cheng et al. [26].

With the increase of surface roughness, the $C_{p\min}$ of the gas tank model in ABL increases from −2.5 to −0.75, which is same as the results in the uniform flow field. Whether the surface roughness is 0.0386 or 0.0771, the $C_{p\min}$ results of this paper are very close to those obtained by Cheng et al. [26].

To sum up, the C_d and $C_{p\min}$ tended to keep constant in high Re region. When $\mathrm{Re} > 6 \times 10^5$, reference wind speed had little effect on the C_d and $C_{p\min}$. The C_d and $C_{p\min}$ of the gas tank had the same trend in uniform flow and turbulent flow field. With the increase of Re, the height of measurement points had little effect on wind pressure distribution of the gas tank. The C_d and $C_{p\min}$ of different measuring layers were gradually approaching in the high Re regime.

In the uniform flow field, the C_d and $C_{p\min}$ of both the smooth and rough surface were close to that of the previous literature. In the ABL turbulent flow field, roughness on the surface promotes the transition of the boundary layer from laminar to turbulent, and the minimum value of C_d increases with increasing k/s.

The turbulence of flow field made the $C_{p\min}$ increase. This phenomenon was most obvious in the smooth surface model. For the smooth surface model, the $C_{p\min}$ increases from −2.7 to −2.3. However, with the increase of surface roughness, the effects of turbulence on $C_{p\min}$ was not significant. For $\gamma = 0.0771$, in both uniform and ABL turbulent flow field, the $C_{p\min}$ was approximately equal to −0.7, which remained basically unchanged.

The C_d and $C_{p\min}$ tended to be stable in high Re region. When $\mathrm{Re} > 0.6 \times 10^6$, reference wind speed had little effect on the C_d and $C_{p\min}$. The C_d and $C_{p\min}$ of the gas tank had the same trend in the uniform flow and turbulent flow field.

With the increase of Re, the height of measurement points had little effect on wind pressure distribution of the gas tank. The C_d and $C_{p\min}$ of different measuring layers were gradually approaching in the high Re regime.

3.1.3. Effect of Reynolds Number on Wind Pressure Coefficient. Figure 10 showed the fluctuating ($C_{p\mathrm{RMS}}$) and mean wind pressure (C_p) distribution along the annular angle of each layer. For space reasons, only the typical height of wind pressure distribution was listed (1440 mm from ground level).

As shown in Figure 10, when the experimental wind speed was greater than 7.6 m/s, the corresponding $\mathrm{Re} > 6 \times 10^5$, the effects of Re on $C_{p\mathrm{RMS}}$ and C_p were limited, which were different from theoretical research about flow around the cylinder. This is because the existence of roughness promotes makes the wind load keep constant.

3.2. Effect of Roughness on Wind Pressure Coefficient. When $\mathrm{Re} > 6 \times 10^5$, the variation of the wind pressure coefficient was not significant. In order to simulate the realistic Re effect, the experimental reference wind speed would be determined to 10.5 m/s (corresponding $\mathrm{Re} \approx 1.0 \times 10^6$), which ensure that the Reynolds number of the flow around the gas tank had been in the supercritical region.

It should be noted that there is an experiment worst point which is always the one at the lowest Re (lowest velocity) when any pressure measurement and any velocity measurement will have the biggest uncertainty as a percentage of that measured value. Because of the definition of C_p, there will be uncertainty in any measured surface pressure which can be quantified by the stated accuracy of the pressure transducer. Often it is stated as X% of the full-scale range of the transducer. Thus, if the transducer can measure a differential pressure up to a stated maximum of 1000 Pa and any measurement is accurate to 0.5% of that value, then any pressure can be measured to the nearest 5 Pa. It means that if, during a measurement, the measured pressure is only 100 Pa, the accuracy will be $+/-(5/100) \times 100\% = 5\%$ of the measured value.

On top of this, there will be a statistical uncertainty based on the total number of samples used to form an average pressure. Usually, in order to ensure the accuracy of data, it is necessary to have enough samples.

3.2.1. Effect of Measurement Point Height on Wind Pressure Coefficient. Figure 11 showed the effects of height of measurement point on the wind pressure coefficient ($C_{p\mathrm{RMS}}$ and C_p) with different surface roughness under reference wind speed (10.5 m/s).

As shown in Figure 11, when the surface roughness of the structure was determined, the $C_{p\mathrm{RMS}}$ and C_p of middle measurement layers of the model were coincident with each other. However, because of the three-dimensional effect, the wind pressure coefficient of the top and bottom measurement layer had a slight deviation. It was found that when the Re of the gas tank model was in the supercritical regime, the height of the measurement layer had little effect on the wind pressure distribution of the gas tank model. Therefore, in the subsequent analysis about the effect of surface roughness on the wind pressure distribution of the gas tank structure, the 8th level ($Z/L = 0.525$) measuring experimental results under reference wind speed (10.5 m/s) was used to analyze the wind load uniformly.

3.2.2. Effect of Spacing Ratio on Wind Pressure Coefficient. If the width of the rough strip increases gradually, the roughness value would be close to the center pitch s, which would lead to form a smooth surface cylinder with a new diameter. In this state, it is obviously not suitable to analyze the effects of roughness on wind pressure distribution without preconditions. Therefore, a new parameter named as spacing ratio would be discussed in this section, by which the applicable condition of roughness effecting the wind pressure distribution would be determined:

$$\lambda = \frac{(s - B)}{s}, \tag{6}$$

where s is the center distance of rough strip and B is the width of the rough strip.

As shown in Figure 12, when $\lambda < 0.9$, the effect of roughness on the wind pressure coefficient was limited. Therefore, experimental data with the spacing ratio greater than 0.9 would be used to investigate the effects of roughness on the wind pressure coefficient on the model surface.

3.2.3. Effects of Ring Reinforcing Strip on Wind Pressure Coefficient. As shown in Figure 13, no matter in the ABL turbulent flow field or uniform flow field, the effects of reinforced strips on the mean wind pressure coefficient was limited. In the test cases, the $C_{p\max}$ for the upwind surface was about 0.95, the $C_{p\min}$ was 0.65, the C_{pb} was -0.39, and the θ_b was basically around 95°. The wind pressure coefficient of the structure was unchanged when the circular reinforcing strip was removed and only the rough condition of the vertical rough strip was present. However, the vertical rough strip conditions were removed, the $C_{p\min}$ had a significant change, from the initial −0.65 to −2.3, the C_{pb} increased slightly to about 0.28, and the θ_b increased to 140°. For the fluctuating wind pressure coefficient, the effects of the reinforcing strip were limited. And the fluctuating wind pressure coefficient was almost coincident under two ceases.

Whether in the ABL turbulent or smooth flow, compared with the column, the ring reinforcement had limited effects on the wind pressure coefficient. So, the impact of ring reinforcement would be ignored.

Based on the abovementioned analysis, the wind tunnel test results with the spacing ratio greater than 0.9 would be analyzed in this section.

Figure 14 showed the $C_{p\max}$ affected by roughness was limited, and its value was about 0.95. However, the effects of roughness on the negative pressure area was significant, the $C_{p\min}$ was 2.3 without roughness, and with an increase of roughness, its value increased to 0.65 significantly. The $\theta_{\min}$ was 90° under the case of the smooth wall, whereas considering the rough case, the angle was about 80°. The θ_b was continuously moved forward with the increase of roughness, the θ_b was shifted from 140° to 90°, and the C_{pb} was reduced from 0.28 to −0.4.

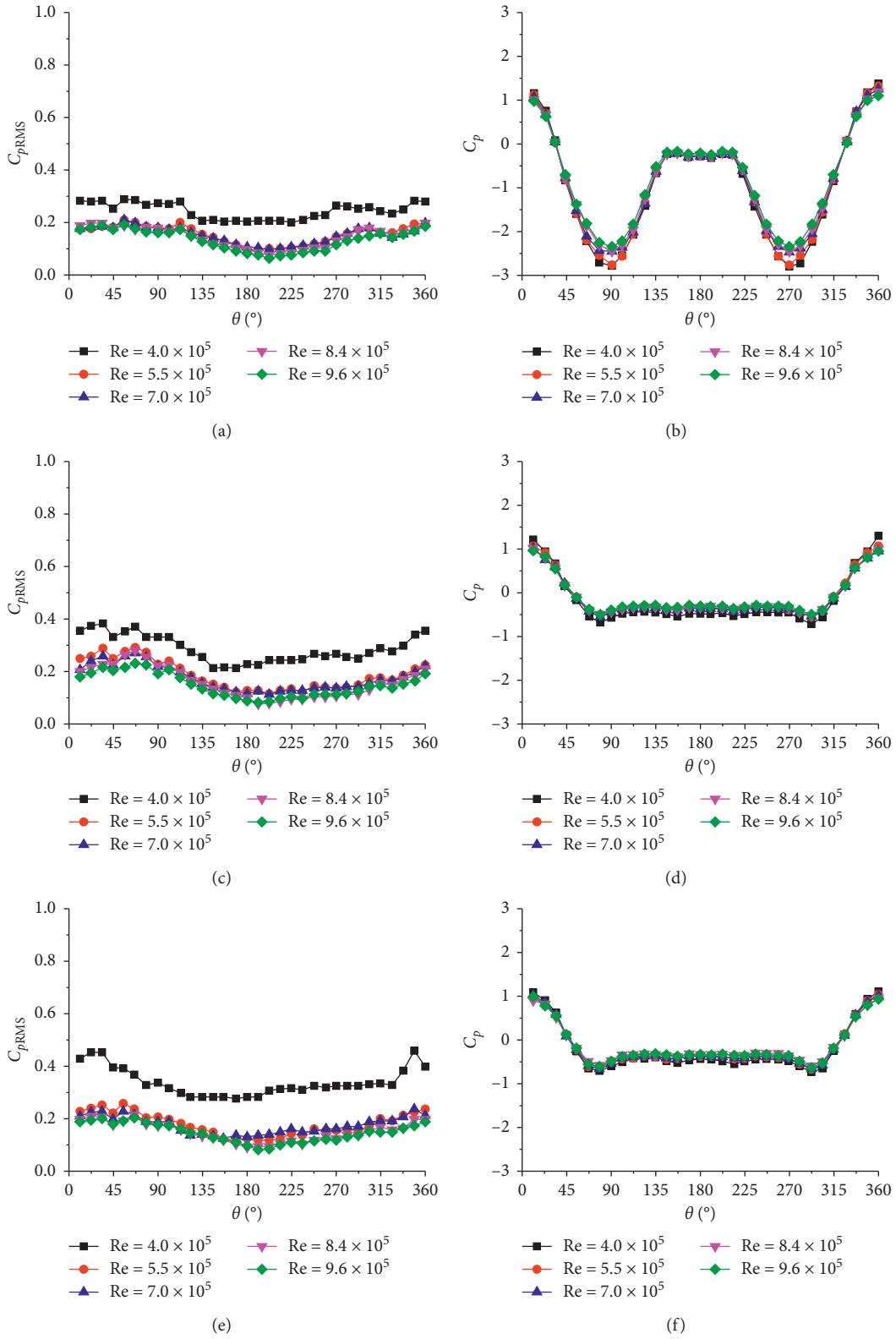

Figure 10: Effect of the Reynolds number on (a, c, e) fluctuating and (b, d, f) local mean wind pressure coefficient. (a, b) $\gamma = 0$, (c, d) $\gamma = 0.0386$, and (e, f) $\gamma = 0.0771$.

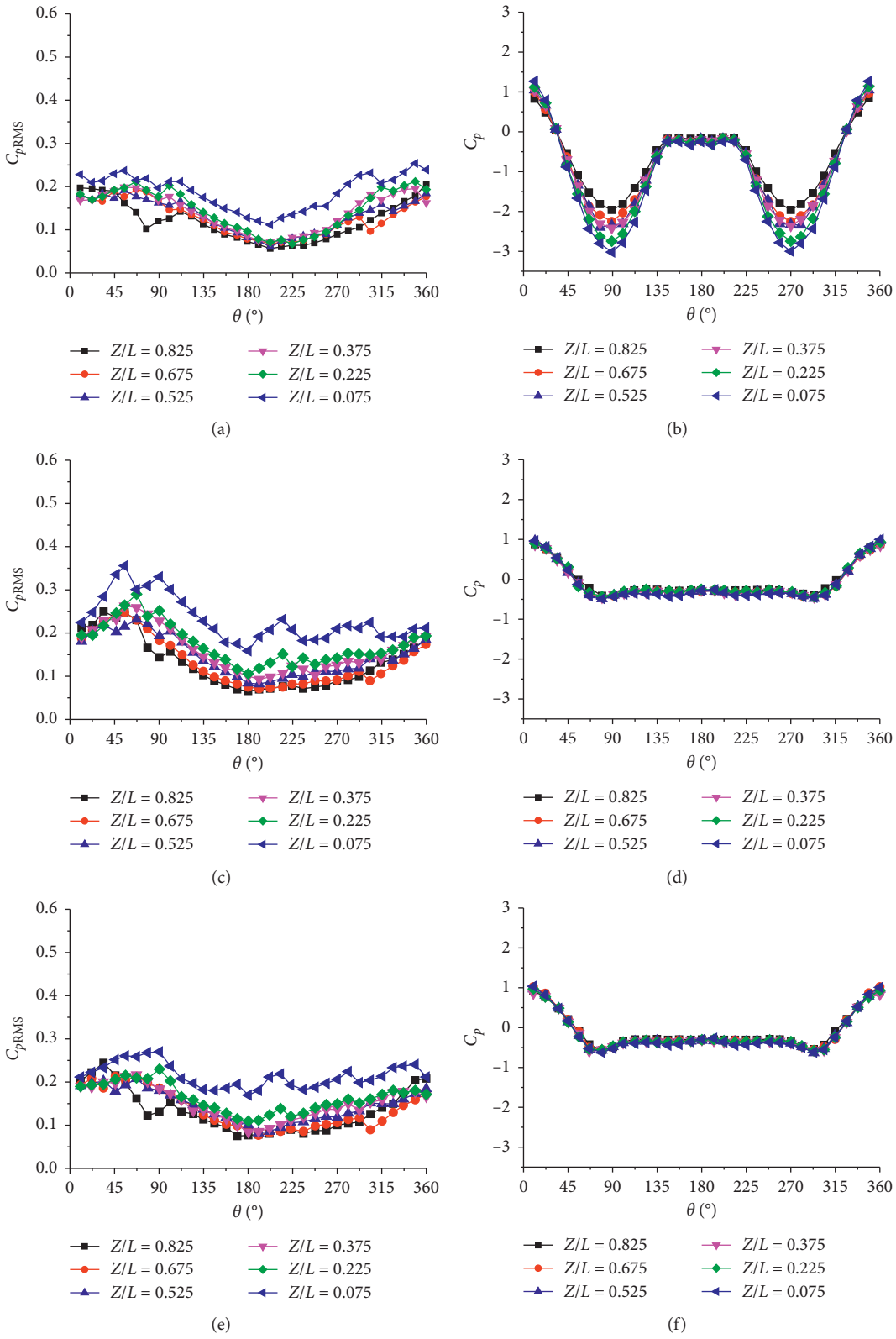

Figure 11: Effect of measurement point height on the fluctuating and local mean wind pressure coefficient. (a, c, e) Type A turbulent flow field and (b, d, f) uniform flow. (a, b) $\gamma = 0$, (c, d) $\gamma = 0.0386$, and (e, f) $\gamma = 0.0771$.

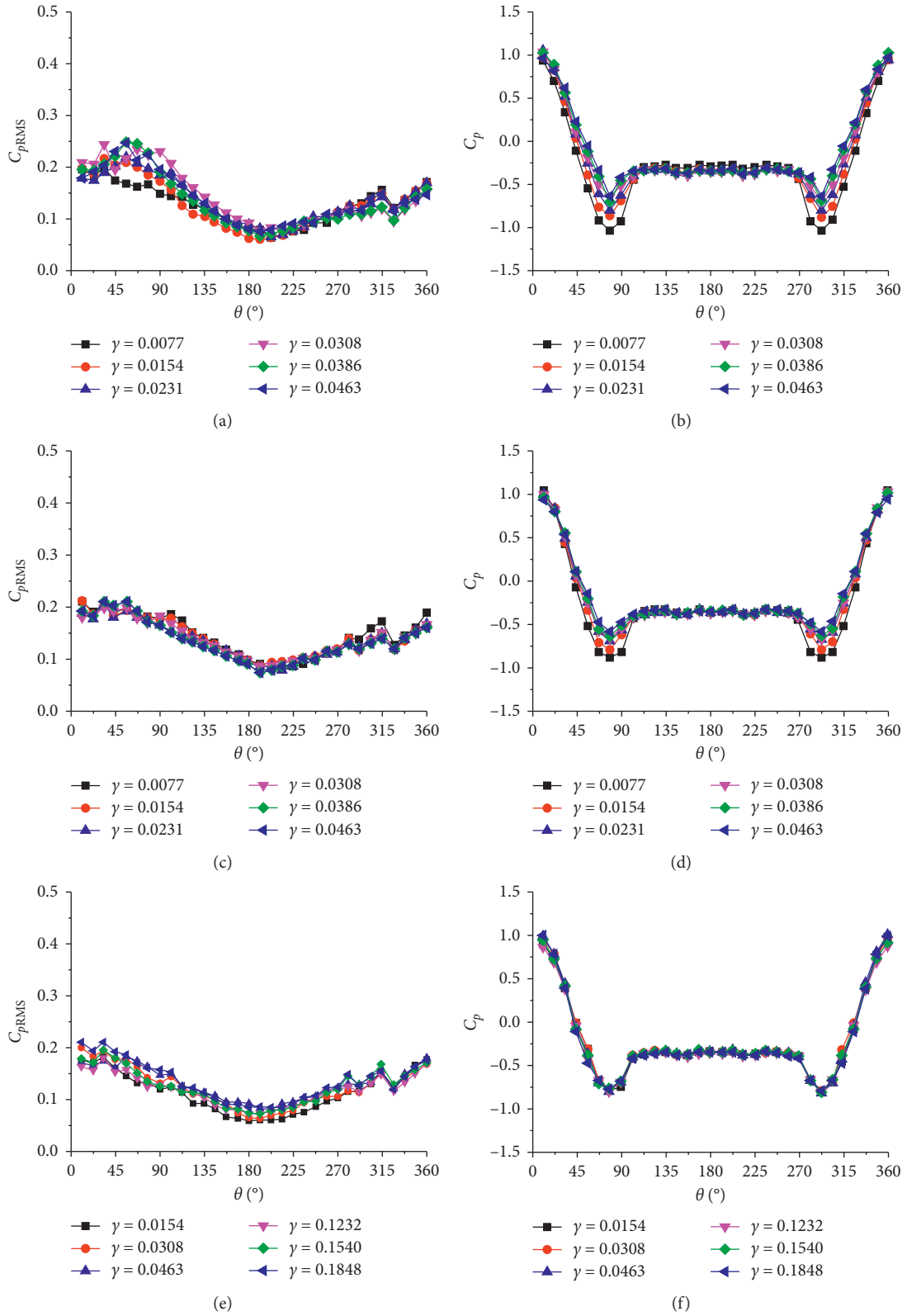

FIGURE 12: Effects of the spacing ratio on wind pressure distribution. (a, c, e) Fluctuating wind pressure coefficient and (b, d, f) mean wind pressure coefficient. (a, b) $\gamma = 0$, (c, d) $\gamma = 0.0386$, and (e, f) $\gamma = 0.0771$.

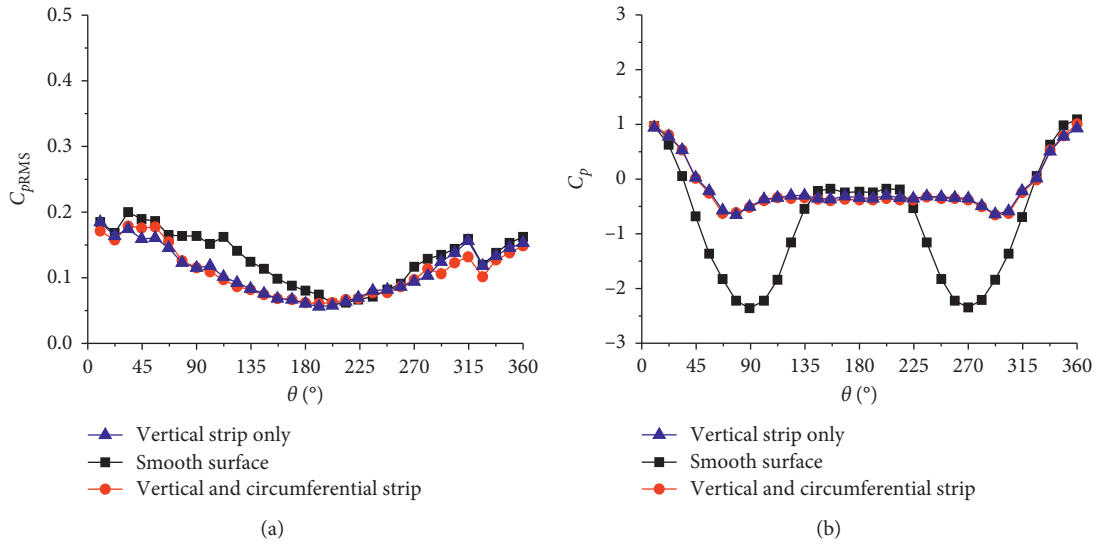

Figure 13: Effects of stiffeners on the wind pressure coefficient: (a) fluctuating wind pressure coefficient and (b) mean wind pressure coefficient.

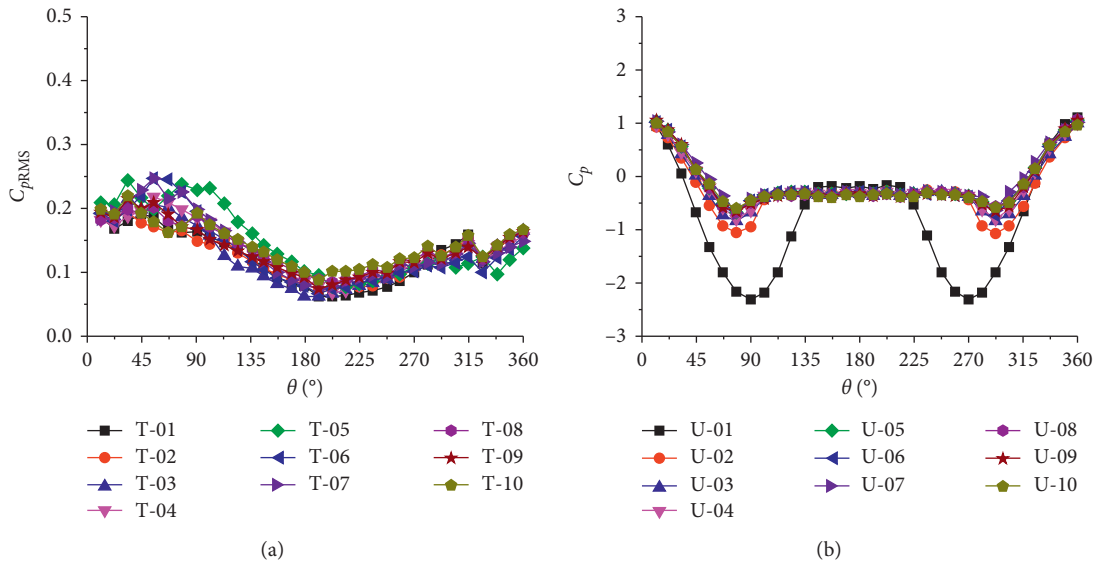

Figure 14: Effects of roughness on wind pressure: (a) fluctuating wind pressure coefficient and (b) mean wind pressure coefficient.

The main parameters of the wind pressure coefficient distribution were listed in Figure 15.

To sum up, with the structural surface roughness increased, the $C_{p\min}$ and C_{pb} increased, and the θ_b constantly reduced. According to Figure 15, the results of $C_{p\min}$ in this paper is larger than those obtained by Zou et al. [25], which may be caused by different structure shape and spacing ratios. The separation angel test results in this paper are consistent with those obtained by Zou et al. [25].

As a result, the increase of roughness makes the gas tank structure wind load distribution tend to be uniform, which was advantageous to wind resistant design.

Figure 16 showed the comparison between the measured data of the wind pressure on the surface of the real gas tank, in which gas tank capacity is 300000 m^3 and the surface roughness is about 0.0772. The figure showed that the measured wind pressure coefficient agrees well with the experiment value.

4. Calculation Method

4.1. Approximate Calculation of Wind Pressure Coefficient of the Gas Cabinet. The main parameters of the wind pressure coefficient [33, 34] were $C_{p\max}$, $C_{p\min}$, C_{pb}, θ_b, and $\theta_{\min}$; through the abovementioned analysis, the effects of

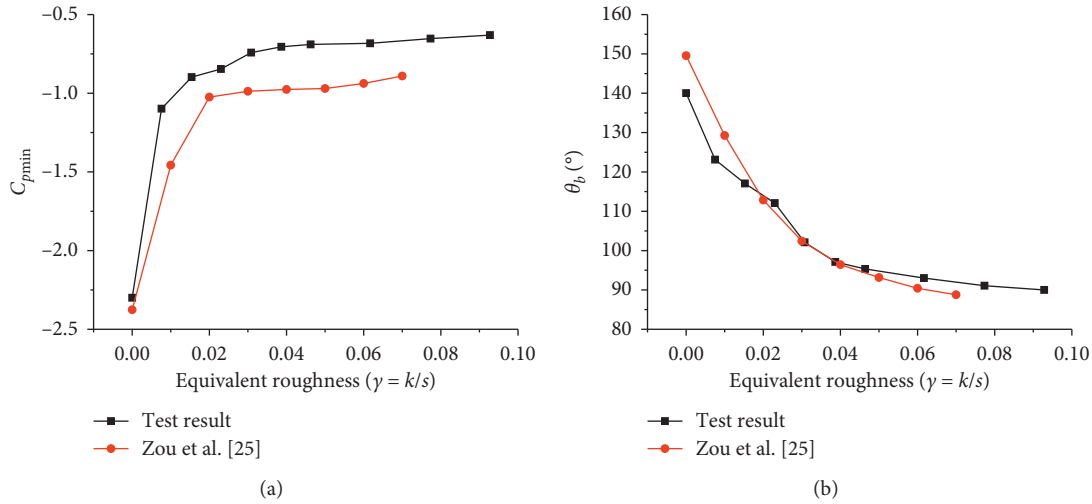

Figure 15: Effects of roughness on $C_{p\min}$ and θ_b: (a) minimum pressure coefficient and (b) azimuthal angle of separation point.

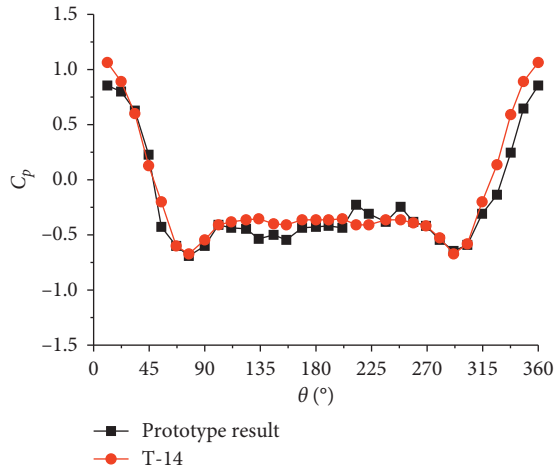

Figure 16: Comparison with the measured value and test value for the wind pressure coefficient.

roughness on the $C_{p\max}$, C_{pb}, and $\theta_{\min}$ was limited. The $C_{p\max}$ was 0.95, the C_{pb} was −0.35, and the $\theta_{\min}$ occurred at 80°.

Based on the test results, the $C_{p\min}$ and the θ_b were fitted by empirical equations (7) and (8), respectively:

$$C_{p\min} = a\gamma^b, \tag{7}$$

where $a = -0.35$ and $b = -0.23$.

$$\theta_b = b + \left(\frac{a-b}{1+(\gamma/c)^d}\right), \tag{8}$$

where $a = 139.49$, $b = 79.76$, $c = 0.02116$, and $d = 1.172$.

Obviously, if the surface is smooth ($\gamma = 0$), it is mathematically meaningless for equation (7), which is not consistent with the results of the flow around a smooth surface cylinder. To ensure the applicability of equation (7), the range of γ should be studied. When $\gamma = 0$, according to the results of flow around a cylinder, the $C_{p\min}$ is about equal to −2.3, which could be used to deduce the applicable range of γ. Therefore, it can be determined that the lower limit value of γ is $3E-4$. In addition, the upper limit value of γ is 0.01. Therefore, in the range of $3E-4 < \gamma < 0.01$, the equation (7) is applicable.

The fitting results were shown in Figure 17. There was some deviation between the results fitted by equations (7) and (8). For minimum pressure coefficient ($C_{p\min}$), due to the limited number of measurement point arranged along the circumference, the real minimum pressure coefficient value may be missed. The fitting uncertainty of θ_b is mainly due to the definition of θ_b. According to Figure 6, θ_b is the angle corresponding to the intersection of two tangent lines which causes some data errors.

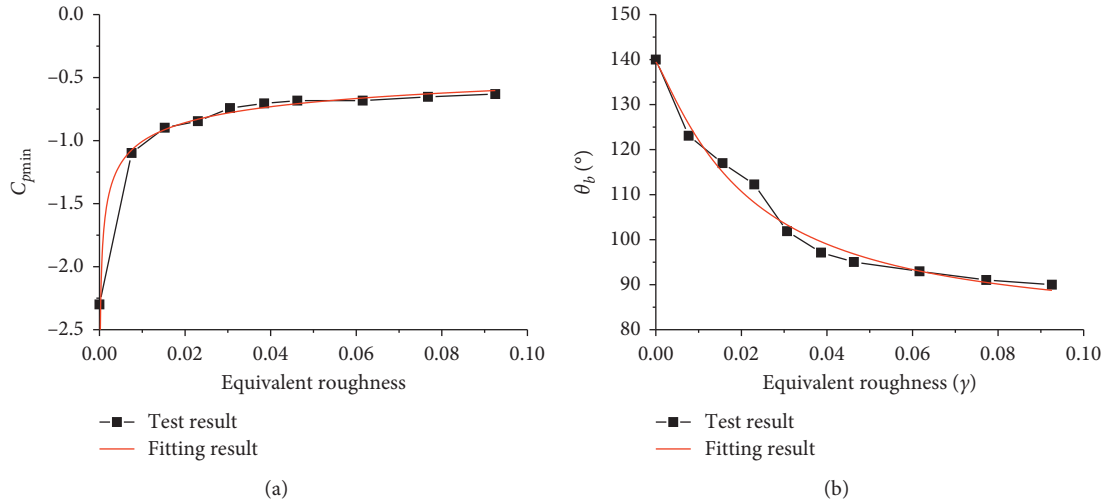

Figure 17: Fitting results of C_{pmin} and θ_b.

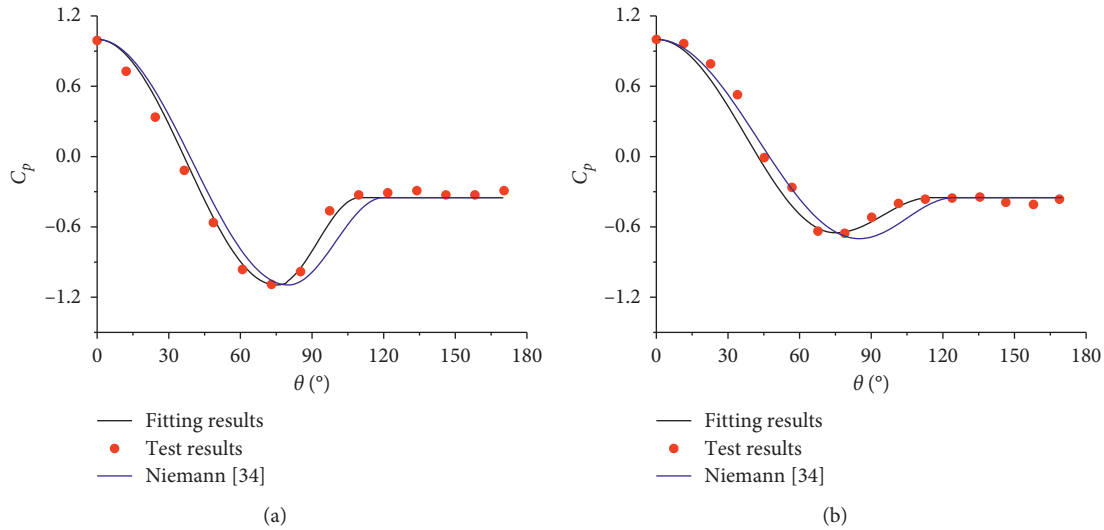

Figure 18: Fitting results of the shape coefficient at different test conditions (a) $\gamma = 0.0386$ and (b) $\gamma = 0.0771$.

Formula (9) was used to estimate the surface mean wind pressure coefficient along the cyclic distribution curve of the gas cabinet. The fitting result was shown in Figure 18.

$$C_p = \begin{cases} C_{pmin} + \left(1 - C_{pmin}\right)\sin^2\left(\dfrac{0.5\pi\left(\theta - \theta_{min}\right)}{\theta_{min}}\right), & 0 < \theta < \theta_{min}, \\ C_{pmin} + \left(C_b - C_{pmin}\right)\sin^2\left(-\dfrac{0.5\pi\left(\theta - \theta_{min}\right)}{\theta_b - \theta_{min}}\right), & \theta_{min} < \theta < \theta_b, \\ C_b, & \theta_b < \theta < \pi. \end{cases} \tag{9}$$

From Figure 18, comparing with the results of the previous literature from Niemann [35], the fitting results proposed by the present article were in good agreement with the experimental values. Therefore, the proposed method of estimating the mean wind pressure coefficient of the gas tank could predict the distribution of the wind pressure coefficient on the gas tank surface.

5. Conclusion

(1) When the Reynolds number of the gas tank was in the supercritical regime, the wind load of the gas tank tended to be stable; the effects of Re on C_d, $C_{p\min}$, $C_{p\mathrm{RMS}}$, and C_p were not significantly. The height of the measuring point had little effect on the wind pressure coefficient.

(2) Based on the definition of the equivalent roughness, it was suggested that the space ratio of roughness greater than 0.9 should be used to analyze the wind pressure coefficient on the gas tank. By comparing the $C_{p\mathrm{RMS}}$ and C_p of the gas tank, the effects of the ring reinforcement on the wind pressure coefficient was limited, which should be ignored.

(3) The effects of roughness on $C_{p\min}$ and θ_b was evident; the $C_{p\min}$ increased from −2.3 to 0.65 with the increase of roughness, and the θ_b moved from 140° to 90°. However, the roughness had limited effect on the $C_{p\max}$, C_{pb}, and $\theta_{\min}$, the value of which was 0.95, −0.35, and 80°, respectively.

(4) By describing the main affecting parameters of the wind pressure coefficient, a wind pressure load model of the gas tank suitable for engineering calculation was proposed. The calculation method could accurately estimate the mean wind pressure coefficient of the gas tank structure.

Nomenclature

a: Fitting parameter
b: Fitting parameter
c: Fitting parameter
B: Width of the rough bar
k: Average height of the rough bar
s: Distance between the rough bar
f: Frequency
$S_v^*(f)$: Normalized wind speed power spectrum
γ: Surface roughness ($=k/s$)
λ: Spacing ratio ($=(s-B)/s$)
ρ: Air density
C_d: Drag coefficient
C_l: Lift coefficient
C_p: Mean wind pressure coefficient
$C_{p\min}$: Minimum pressure coefficient
$C_{p\max}$: Maximum pressure coefficient
C_{pb}: Pressure coefficient within the base region of the model
$C_{p\mathrm{RMS}}$: Fluctuating wind pressure coefficient
D: Diameter of the gas tank model
H: Height of the gas tank
Z: Height of the measurement point
L: Total height of the gas tank model
θ: Azimuthal angle of the measurement point
θ_b: Azimuthal angle of the separation point
$\theta_{\min}$: Azimuthal angle of the minimum pressure coefficient
$p_\infty(z)$: Freestream static pressure
$V_\infty(z)$: Oncoming wind velocity at height Z
Re: Reynolds number
R_{ec}: Reynolds number corresponding to critical regime
St: Strouhal number

Data Availability

The data used to support the findings of this study are included within the article.

Conflicts of Interest

The authors declare that they have no conflicts of interest.

References

[1] N. Su, S. Peng, and N. Hong, "Analyzing the background and resonant effects of wind-induced responses on large-span roofs," *Journal of Wind Engineering and Industrial Aerodynamics*, vol. 183, pp. 114–126, 2018.

[2] C. Wieselsberger, *New Data on the Laws of Fluid Resistance*, National Advisory Committee for Aeronautics, Washington, DC, USA, 1922.

[3] G. Schewe, "On the force fluctuations acting on a circular cylinder in crossflow from subcritical up to transcritical Reynolds numbers," *Journal of Fluid Mechanics*, vol. 133, no. 1, pp. 265–285, 1983.

[4] C. H. K. Williamson, "Oblique and parallel modes of vortex shedding in the wake of a circular cylinder at low Reynolds numbers," *Journal of Fluid Mechanics*, vol. 206, no. 1, pp. 579–627, 1989.

[5] A. Roshko, "Experiments on the flow past a circular cylinder at very high Reynolds number," *Journal of Fluid Mechanics*, vol. 10, no. 3, pp. 345–356, 1961.

[6] C. Norberg, "Fluctuating lift on a circular cylinder: review and new measurements," *Journal of Fluids and Structures*, vol. 17, no. 1, pp. 57–96, 2003.

[7] C. Demartino and F. Ricciardelli, "Aerodynamics of nominally circular cylinders: a review of experimental results for civil engineering applications," *Engineering Structures*, vol. 137, pp. 76–114, 2017.

[8] G. Eiffel, "On the resistance of spheres in air motion," *Comptes Rendus de l'Académie des Sciences*, vol. 155, p. 1597, 1912.

[9] S. G. I. Taylor, "Pressure distribution around the cylinder," *Advisory Committee of Aeronautics*, vol. 191, 1916.

[10] A. Fage and F. C. Johansen, "XLII. The structure of vortex sheets," *The London, Edinburgh, and Dublin Philosophical Magazine and Journal of Science*, vol. 5, no. 28, pp. 417–441, 1928.

[11] B. J. Cantwell, *An experimental study of turbulent near-wake of a circular cylinder at Re = 140000*, Ph.D. thesis, California Institute of Technology, Pasadena, CA, USA, 1976.

[12] A. I. Korotkin, "The three dimensionality of the flow transverse to a circular cylinder," *Fluid Mechanics Soviet Research*, vol. 5, pp. 96–103, 1976.

[13] L. V. Schmidt, "Measurement of fluctuating air loads on a circular cylinder," *Journal of Aircraft*, vol. 2, no. 1, pp. 49–55, 1965.

[14] A. M. Jones and J. G. Knudsen, "Drag coefficients at low Reynolds numbers for flow past immersed bodies," *AIChE Journal*, American Institute of Chemical Engineers, vol. 7, no. 1, pp. 20–25, 1961.

[15] K. A. Warschauer and J. A. Leene, "Experiments on mean and fluctuating pressures of circular cylinders at cross flow at very high Reynolds numbers," in *Proceedings of the International Conference on Wind Effects on Buildings and Structures*, pp. 305–315, Tokyo, 1971.

[16] E. Achenbach, "Distribution of local pressure and skin friction around a circular cylinder in cross-flow up to $\mathrm{Re} = 5 \times 106$," *Journal of Fluid Mechanics*, vol. 34, no. 4, pp. 625–639, 1968.

[17] P. W. Bearman, "On vortex shedding from a circular cylinder in the critical Reynolds number régime," *Journal of Fluid Mechanics*, vol. 37, no. 3, pp. 577–585, 1969.

[18] E. Achenbach, "Influence of surface roughness on the cross-flow around a circular cylinder," *Journal of Fluid Mechanics*, vol. 46, no. 2, pp. 32–37, 1971.

[19] A. Fage and J. Warsap, "The effects of turbulence and surface roughness on the drag of a circular cylinder," *Aeronautical Research Committee Report and Memoranda*, vol. 1283, 1929.

[20] G. Buresti, "The effect of surface roughness on the flow regime around circular cylinders," *Journal of Wind Engineering Industrial Aerodynamics*, vol. 8, no. 1-2, pp. 105–114, 1981.

[21] M. M. Zdravkovich, "Conceptual overview of laminar and turbulent flows past smooth and rough circular cylinders," *Journal of Wind Engineering and Industrial Aerodynamics*, vol. 33, no. 1-2, pp. 53–62, 1990.

[22] J. L. D. Ribeiro, "Effects of surface roughness on the two-dimensional flow past circular cylinders *i*: mean forces and pressures," *Journal of Wind Engineering and Industrial Aerodynamics*, vol. 37, no. 3, pp. 299–309, 1991.

[23] M. M. Zdravkovich, "Flow around circular cylinders," *Fundamentals*, vol. 1, no. 1, p. 216, 2003.

[24] E. Achenbach and E. Heinecke, "On vortex shedding from smooth and rough cylinders in the range of Reynolds numbers 6×10^3 to 5×10^6," *Journal of Fluid Mechanics*, vol. 109, no. 5, pp. 239–251, 2006.

[25] Y. F. Zuo, X. H. He, H. F. Wang, L. X. Tan, and H. W. Niu, "Influence of modal surface roughness on wind pressure distribution of hyperbolic cooling tower," *Journal of Hunan University (Natural Science)*, vol. 42, no. 7, pp. 16–24, 2015.

[26] X. Cheng, L. Zhao, Y. Ge, R. Dong, and C. Dong, "Wind effects on rough-walled and smooth-walled large cooling towers," *Advances in Structural Engineering*, vol. 20, no. 6, pp. 843–864, 2017.

[27] Z. L. Li, X. P. Liu, Z. T. Yan, W. H. Jiao, and D. K. Yu, "Analysis of dynamic characteristic and identification of natural modes with significant contributions to wind-induced vibration of MAN type dry gas storage tank," *Journal of Vibration and Shock*, vol. 34, no. 19, pp. 79–86, 2015.

[28] X. P. Liu, Z. L. Li, Z. T. Yan, and J. F. Chen, "Full aeroelastic model design and modal test for MAN type dry gas," *Journal of Southwest Jiaotong University*, vol. 51, no. 4, pp. 1–6, 2016.

[29] J. F. Yao, W. J. Lou, G. H. Shen et al., "Influence of inflow turbulence on the flow characteristics around a circular cylinder," *Applied Sciences*, vol. 9, no. 3595, pp. 1–20, 2019.

[30] L. Qingkuan, S. Qi, Z. Yunfei, L. Conghui, M. Wenyong, and L. Xiaobing, "Experimental study on Reynolds number effect on aerodynamic pressure and forces of cylinder," *Journal of Experiments in Fluid Mechanics*, vol. 30, pp. 7–13, 2016, in Chinese.

[31] O. Güven, C. Farell, and V. C. Patel, "Surface-roughness effects on the mean flow past circular cylinders," *Journal of Fluid Mechanics*, vol. 98, no. 4, pp. 673–701, 1980.

[32] J. W. G. Van Nunen, A. J. Persoon, and H. Tijdeman, "Pressures and forces on a circular cylinder in a cross flow at high Reynolds numbers," in *Proceedings of the IUTAM/IAHR Symposium on Flow-Induced Structural Vibrations*, Springer, Karlsruhe, Germany, August 1974.

[33] S. G. Liang, L. H. Zou, and L. Zhao, "The investigation of 3-D dynamic wind loads on lattice towers by wind tunnel test," *Acta Aerodynamica Sinica*, vol. 03, pp. 311–318+329, 2007.

[34] S. G. Liang, L. H. Zou, and L. Zhao, "Analytical model of dynamic wind loads on lattice towers," *Journal of Tongji University (Natural Science)*, vol. 02, pp. 166–171, 2008.

[35] H. J. Niemann, "Wind effects on cooling-tower shells," *Journal of the Structural Division*, vol. 106, pp. 643–661, 1980.